PCCP

PAPER

View Article Online
View Journal | View Issue

Cite this: *Phys. Chem. Chem. Phys.*, 2015, **17**, 29184

On the origin of preferred bicarbonate production from carbon dioxide (CO_2) capture in aqueous 2-amino-2-methyl-1-propanol (AMP)†

Haley M. Stowe,[a] Linas Vilčiauskas,[b] Eunsu Paek[b] and Gyeong S. Hwang*[ab]

Received 16th August 2015,
Accepted 7th October 2015

DOI: 10.1039/c5cp04876a

www.rsc.org/pccp

AMP and its blends are an attractive solvent for CO_2 capture, but the underlying reaction mechanisms still remain uncertain. We attempt to elucidate the factors enhancing bicarbonate production in aqueous AMP as compared to MEA which, like most other primary amines, preferentially forms carbamate. According to our predicted reaction energies, AMP and MEA exhibit similar thermodynamic favorability for bicarbonate versus carbamate formation; moreover, the conversion of carbamate to bicarbonate also does not appear more favorable kinetically in aqueous AMP compared to MEA. *Ab initio* molecular dynamics simulations, however, demonstrate that bicarbonate formation tends to be kinetically more probable in aqueous AMP while carbamate is more likely to form in aqueous MEA. Analysis of the solvation structure and dynamics shows that the enhanced interaction between N and H_2O may hinder CO_2 accessibility while facilitating the AMP + H_2O → $AMPH^+$ + OH^- reaction, relative to the MEA case. This study highlights the importance of not only thermodynamic but also kinetic factors in describing CO_2 capture by aqueous amines.

I. Introduction

Carbon dioxide (CO_2) removal from flue gas has become increasingly important due to global climate change concerns.[1] Aqueous alkanolamines are frequently used as solvents for absorption/stripping which is an economically well-suited process for CO_2 capture and sequestration.[2] Monoethanolamine (MEA) is one of the most widely used and studied alkanolamines, but its expansion for commercial use tends to be limited due to degradation problems and high parasitic energy consumption during solvent regeneration.[3,4] 2-Amino-2-methyl-1-propanol (AMP) and other sterically hindered primary amines have been suggested as an alternative because they exhibit both high CO_2 loading capacities and relatively fast absorption rates, in addition to low degradation and corrosion rates.[5–8] However, the mechanism underlying the reaction between CO_2 and aqueous AMP still remains controversial.

It is now well adopted that CO_2 capture by most primary amines including MEA in an aqueous solution takes place *via* a two-step mechanism involving a zwitterion intermediate.[9,10] The zwitterion may subsequently undergo deprotonation by another amine to form a carbamate ion and a protonated amine, leading to a loading capacity of 0.5 mol CO_2 per mol amine. Conversely, the primary products of the reaction of aqueous AMP with CO_2 have been found to be bicarbonate (HCO_3^-) and protonated AMP ($AMPH^+$), with carbamate ($AMPCOO^-$) but whose concentration is about an order of magnitude lower than HCO_3^-.[11] It is also known that bicarbonate formation predominantly takes place in aqueous tertiary amines such as methyldiethanolamine (MDEA), yielding the theoretical maximum capacity of 1 mol CO_2 per mol amine.[12] In the tertiary amine system, bicarbonate can be formed by the base-catalyzed hydration of CO_2, *e.g.*, MDEA + H_2O + CO_2 → $MDEAH^+$ + OH^- + CO_2 → $MDEAH^+$ + HCO_3^-.[13]

However, according to previous experimental observations, the absorption rate of CO_2 in aqueous AMP tends to be about two orders of magnitude faster as compared to the MDEA case.[14] On the basis of this significant rate difference, it has also been speculated that CO_2 may first be captured by AMP to form a carbamate ion ($AMPCOO^-$), but the carbamate could be unstable and thus undergo subsequent hydrolysis to form bicarbonate, *i.e.*, $AMPCOO^-$ + H_2O → HCO_3^- + $AMPH^+$.[5,15] In addition, decomposition of the zwitterion to bicarbonate has been proposed as another alternative mechanism, *i.e.*, AMP^+COO^- + H_2O → HCO_3^- + $AMPH^+$.[5,16] While the underlying mechanism of CO_2 capture by AMP remains highly debatable, recent first-principles density functional theory (DFT) calculations have

[a] *Materials Science and Engineering Program, University of Texas at Austin, Austin, Texas 78712, USA. E-mail: gshwang@che.utexas.edu; Fax: +1-512-471-7060; Tel: +1-512-471-4847*

[b] *McKetta Department of Chemical Engineering, University of Texas at Austin, Austin, Texas 78712, USA*

† Electronic supplementary information (ESI) available. See DOI: 10.1039/c5cp04876a

demonstrated the possibility of forming zwitterionic intermediates and carbamate ions from the reaction of CO_2 with aqueous AMP.[17–21] However, previous theoretical studies have also predicted that the activation barriers for the hydrolysis conversion of both AMP and MEA carbamate to bicarbonate are high and also comparable,[18–20] implying that not only $MEACOO^-$ but also $AMPCOO^-$ are relatively stable and may not easily undergo the hydrolysis reaction to form HCO_3^-. This gives a hint that preferred bicarbonate formation in the AMP–H_2O–CO_2 system might not be due to carbamate being less stable than the MEA case.

In this work, we investigate the factors underlying the preferred production of bicarbonate over carbamate from CO_2 absorption in aqueous AMP, with comparison to the MEA case where carbamate is predominantly formed. First, we evaluate the thermodynamic favorability of carbamate and bicarbonate formation in the AMP/MEA–H_2O–CO_2 system using *ab initio* molecular dynamics (AIMD) (with explicit solvent) and static quantum mechanical (QM) (with implicit solvent) calculations. We also perform AIMD simulations to identify likely elementary reactions. Then, we attempt to explain the different CO_2 capture mechanisms observed between aqueous AMP and MEA by analyzing the electronic structure of amines as well as the local arrangement and dynamics of solvent molecules using combined QM and classical force field calculations. The improved understanding of CO_2 absorption mechanisms in amine-based solutions provides valuable guidance on how to design new high-performance solvent materials.

II. Computational methods

A. Quantum mechanical calculation

We performed AIMD simulations within the Born–Oppenheimer approximation using the Vienna Ab initio Simulation Package (VASP).[22] The projector augmented wave (PAW) method with a planewave basis set and the Perdew–Burke–Ernzerhof generalized gradient approximation (GGA-PBE)[23] were employed. An energy cutoff of 400 eV was applied for planewave expansion of the electronic eigenfunctions. Only the gamma point was sampled for Brillouin zone integration. Simulations were run in the canonical (*NVT*) or microcanonical (*NVE*) ensemble as specified after equilibrating the system using classical MD.

We used the Gaussian 09 suite of programs[24] for the static QM calculations at the B3LYP/6-311++G(d,p) level of theory. The SMD model of Truhlar and co-workers[25] within the polarizable continuum model (PCM) approach was used to estimate the solvation enthalpies and free energies of all species. The vibrational contributions to the free energy were estimated using the harmonic frequency analysis.

B. Classical molecular dynamics simulation

Classical MD simulations were performed using the Large-scale Atomic/Molecular Massively Parallel Simulator (LAMMPS) program.[26] We used a modified AMBER force field[27,28] for MEA and AMP with the SPC/E water model[29] and a flexible version of the EPM2 force field for CO_2.[30,31] We obtained the atomic charges for MEA and AMP from QM calculations at the B3LYP/6-311++G(d,p) level of theory and using the restrained electrostatic potential (RESP) procedure.[32] The force field parameters for AMP, MEA, and CO_2 are included in the ESI.† All bonds involving H atoms were constrained using the SHAKE algorithm.[33] Spherical cutoffs of 10 Å and 12 Å were used for the Lennard-Jones and Coulomb interactions, respectively. Electrostatic interactions beyond the cutoff were calculated using the Ewald summation method.[34] Simulations were run in the *NVT* ensemble with the temperature controlled by a Nosé–Hoover thermostat[35] with a 100 fs damping parameter. Each simulated system was first annealed at 1000 K and then quenched to 323 K, followed by another anneal and quench cycle. Production runs were carried out for 1 ns with a timestep of 1 fs.

III. Results and discussion

A. Thermodynamic favorability of bicarbonate and carbamate formation

We first calculated and compared the changes of total energy (ΔE) in the reactions of aqueous AMP (or MEA) with CO_2 to form carbamate or bicarbonate using AIMD simulations at 313 K; while typical operating temperatures for CO_2 capture by aqueous amines are between 40–60 °C (313–333 K),[3–5] the relatively low temperature was used to minimize any unwanted reaction events. For 30 wt% AMP (MEA) with a loading of 0.5 mol CO_2 per mol amine, 2 AMP (MEA), 1 CO_2 and 30 (16) H_2O molecules were placed in a cubic simulation box of edge length 10.83 Å (8.774 Å) with periodic boundary conditions. Then, CO_2 was assumed to undergo a reaction to form carbamate [2AMP (or MEA) + CO_2 → $AMPCOO^-$ + $AMPH^+$ (or $MEACOO^-$ + $MEAH^+$)] or bicarbonate [AMP (or MEA) + CO_2 + H_2O → $AMPH^+$ (or $MEAH^+$) + HCO_3^-]. For each reacted/unreacted system, five different samples were considered to estimate its average total energy. Illustrations of the molecules considered and the system compositions are included in the ESI.†

As summarized in Table 1, the carbamate and bicarbonate formation reactions are both predicted to be exothermic with ΔE of about −17 (−15) kcal mol^{-1} CO_2 and −22 (−20) kcal mol^{-1} CO_2, respectively, for the case of 30 wt% AMP (MEA). Although the predicted ΔE are rather widely scattered because of the small sample sizes employed, our AIMD results unequivocally suggest that both reactions forming bicarbonate and carbamate are thermodynamically favorable, with similar ΔE values. Previous experiments also reported that the reactions of CO_2 with 30 wt% AMP and MEA yield enthalpy changes (ΔH) of about −18 kcal mol^{-1}

Table 1 Predicted energy changes (ΔE in kcal mol^{-1}) from AIMD simulations at 313 K for carbamate (2**X** + CO_2 → **X**H^+ + **X**COO^-) and bicarbonate (**X** + H_2O + CO_2 → **X**H^+ + HCO_3^-) formation reactions for **X** = AMP and MEA (in parenthesis) in 30 wt% aqueous solution

Reaction [**X** = AMP (MEA)]	ΔE
2**X** + CO_2 → **X**H^+ + **X**COO^-	−17.1 ± 6.9 (−15.0 ± 3.5)
X + H_2O + CO_2 → **X**H^+ + HCO_3^-	−22.3 ± 7.7 (−19.5 ± 3.1)

CO_2[36] and −21 kcal mol^{-1} CO_2,[37] respectively. The experimental measurements show reasonable agreement with our predictions although these exothermic enthalpy changes may also include the hydration enthalpy of CO_2 (which is however only −4.3 kcal mol^{-1} in an infinitely diluted aqueous solution[38]).

For comparison, we also evaluated the reaction energetics using an implicit solvent model. The changes in enthalpy and Gibbs free energy in the aqueous phase (ΔH°_{aq}, ΔG°_{aq}) were calculated using the standard thermodynamic cycles where the gaseous energy changes (ΔG°_{gas}(react → prod)) were corrected for a difference in solvation energies ($\Delta\Delta G^\circ_{solv}$(react → prod)). More details regarding the computational approach, and the predicted enthalpy and free energies of the individual species are included in the ESI.† The estimated (ΔH°_{aq}, ΔG°_{aq}) for various reactions are reported in Table 2.

The implicit solvent calculations predict the bicarbonate and carbamate formation reactions to yield ΔH of −5.72 (−3.59) kcal mol^{-1} and −5.31 (−7.50) kcal mol^{-1} for AMP (MEA) in aqueous solution, respectively. The result also confirms that bicarbonate formation is energetically comparable to carbamate formation in both aqueous AMP and MEA cases.

It is also worthwhile to note that the predicted ΔH from QM calculations are much smaller in magnitude than those from previous experimental measurements and aforementioned AIMD calculations; note that the ΔE from AIMD is close to the ΔH [= ΔE + Δ(PV)] from experiments while the PV work is negligible in the aqueous amine systems considered. This may suggest that there would be strong solvation effects which may not be adequately described by the implicit solvent method. In fact, the inclusion of explicit H_2O molecules in the implicit solvent has been found to more accurately estimate the pK_a of HCO_3^- [39] and also alter the relative favorability between bicarbonate and carbamate formation in amine–CO_2 systems.[19] Moreover, other previous studies[40,41] have shown that AIMD simulations including the solvent environment explicitly can predict more accurately the free energy difference and barrier for the OH^- + CO_2 → HCO_3^- reaction in aqueous solution when compared with continuum solvent models, emphasizing the importance of solvation structure and dynamics in predicting the reaction pathway and energetics.

When comparing ΔG°_{aq} from the implicit solvent calculations, carbamate formation is only marginally (2.35 kcal mol^{-1}) more favorable than bicarbonate formation for MEA, whereas AMP tends to energetically favor bicarbonate formation by 2.28 kcal mol^{-1}; our results are generally consistent with previous theoretical studies,[17–20,42,43] although the reported ΔH and ΔG are scattered depending on the reference states used. Nonetheless, the predicted energetics would be susceptible to a number of errors stemming from the inability of the continuum approach to accurately describe the solvation of charged products as well as the assumption of infinite dilution and the absence of interactions between charged products at moderate amine concentrations employed in typical experimental settings.

In the thermodynamics point of view, the relative concentration of carbamate over bicarbonate can be determined in terms of its thermodynamic favorability with respect to bicarbonate. However, the direct conversion from carbamate to bicarbonate, *i.e.*, $AMPCOO^-$ ($MEACOO^-$) + H_2O → HCO_3^- + $AMPH^+$ ($MEAH^+$), for both systems are predicted to be comparable and relatively high (∼37 kcal mol^{-1});[18,20] this is in contradiction to previous suggestions that $AMPCOO^-$ is rather unstable relative to $MEACOO^-$ due to the steric hindrance by the two large CH_3 groups such that the carbamate more easily undergoes hydrolysis to form bicarbonate in comparison to the MEA case.[5,15] We also performed AIMD simulations at very high temperatures (∼1000 K), but $AMPCOO^-$ remained intact for 100 ps while the proton transfer reaction between $AMPH^+$ and AMPCOOH occurred. Since the simulation time is limited, this does not mean that $AMPCOO^-$ cannot convert to HCO_3^-, but at least suggests that $AMPCOO^-$ would not be such an unstable product; this can be supported by the fact that CO_2 is strongly bound to the N of both AMP and MEA in the carbamate form (note the similar N–C distances in Fig. S1, ESI†). Although AMP carbamate may eventually undergo hydrolysis to form bicarbonate, it might take too long to reach thermodynamic equilibrium at moderate temperatures. Furthermore, the energy barriers for the interconversion between carbamate and bicarbonate tend to be quite similar in aqueous AMP and MEA as predicted by previous calculations;[18,20] it does not appear that the hydrolysis reaction would happen more quickly for $AMPCOO^-$ relative to $MEACOO^-$. Therefore, the relative concentrations of carbamate and bicarbonate could not be predicted only by their thermodynamic favorability. Given that, another possible factor is that either carbamate or bicarbonate formation would be kinetically preferred in aqueous AMP (and MEA). Next, we will examine and discuss the kinetics aspect.

B. Reaction dynamics in AMP/MEA–H_2O–CO_2 from AIMD

AIMD simulations were performed to examine possible pathways for CO_2 reaction with aqueous MEA and AMP. For the aqueous AMP system, $30H_2O$, 2AMP, and $1CO_2$ molecules, corresponding to 30 wt% aqueous AMP with CO_2, were placed in a cubic simulation box of edge length 10.62 Å with periodic boundary conditions. The simulations were carried out in the

Table 2 Predicted enthalpy (ΔH) and free energy (ΔG) changes in kcal mol^{-1} using static QM calculations at a theory level of B3LYP/6-311++G(d,p) for carbamate (2**X** + CO_2 → **X**H^+ + **X**COO^-) and bicarbonate (**X** + H_2O + CO_2 → **X**H^+ + HCO_3^-) formation reactions for **X** = AMP and MEA (in parenthesis) in the gas-phase and aqueous solution (with an implicit solvent model) as indicated

Reaction [**X** = AMP (MEA)]	ΔH°_{gas}	ΔG°_{gas}	$\Delta\Delta H^\circ_{solv}$	$\Delta\Delta G^\circ_{solv}$	ΔH°_{aq}	ΔG°_{aq}
2**X** + CO_2 → **X**H^+ + **X**COO^-	129.47 (133.11)	139.63 (142.74)	−134.78 (−140.61)	−135.86 (−141.32)	−5.31 (−7.50)	3.76 (1.42)
X + H_2O + CO_2 → **X**H^+ + HCO_3^-	125.88 (132.53)	135.27 (141.81)	−131.59 (−136.13)	−133.79 (−138.04)	−5.72 (−3.59)	1.48 (3.77)

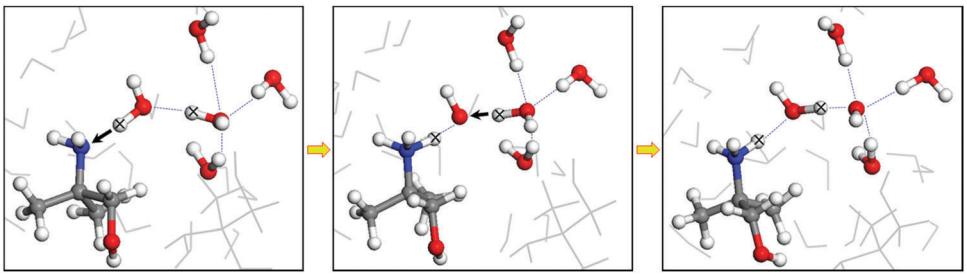

Fig. 1 Snapshots from AIMD simulations of 30 wt% aqueous AMP with CO_2 at 400 K, demonstrating the occurrence of AMP + H_2O → $AMPH^+$ + OH^- reaction and subsequent OH anion (OH^-) diffusion. System contains $30H_2O$, 2AMP and $1CO_2$ molecules in a cubic periodic box with side length of 10.62 Å. The white, grey, blue and red balls represent H, C, N and O atoms, respectively, and the protons and hydrogen atom involved in the proton transfer reaction are also indicated by x. Other H_2O and AMP molecules in the system are also shown in 'grey' line format.

NVT ensemble at 400 K (somewhat above typical absorber temperatures of 313–333 K [3–5]); the relatively high temperature was used in order to speed up reactions so as to identify probable elementary events occurred during the limited simulation time span. This approach would be appropriate, as rationalized in our previous work.[44] During about 120 ps of simulation, we observed only the AMP + H_2O → $AMPH^+$ + OH^- reaction, as illustrated in Fig. 1; this reaction occurred in 7 out of 10 cases with different initial configurations. The OH^-, coordinated by 4 H_2O molecules, is found to travel through H-bonded networks in water; the predicted diffusion behavior of OH^- is consistent with previous theoretical studies.[45] The OH^- may react with CO_2 to form bicarbonate, *i.e.*, OH^- + CO_2 → HCO_3^-. This reaction has been predicted to require overcoming a relatively large barrier (~10 kcal mol^{-1})[40,41] in an aqueous medium due to the rather strong solvation of OH^-; the OH^- solvation shell can be significantly disrupted by the presence of amines at high concentrations, thereby facilitating the bicarbonate formation as demonstrated in Fig. S2 (ESI†). Previous studies also suggest amines can act like a catalyst to facilitate bicarbonate formation,[13,46] although the underlying reasons warrant further investigation.

For the case of 25 wt% aqueous MEA with CO_2 (where $20H_2O$, 2MEA, and $1CO_2$ molecules were placed in a cubic periodic box with side length of 9.278 Å), MEA is likely to undergo the reaction with CO_2 to form $MEACOO^-$ and $MEAH^+$, *i.e.*, 2MEA + CO_2 → $MEACOO^-$ + $MEAH^+$ according to our previously reported AIMD simulations at 400 K.[44] As seen in Fig. S3 in the ESI,† CO_2 attaches to the N of MEA to form the zwitterionic adduct, MEA^+COO^- [(a)], followed by proton release to form $MEACOO^-$ [(b)]. The proton travels through the water network, until abstracted by another MEA to form $MEAH^+$ [(c)].

The AIMD results may suggest that carbamate formation would be more likely in aqueous MEA while the route to bicarbonate formation would be kinetically more probable in aqueous AMP. In the following sections, we will present possible underlying reasons for the difference between MEA and AMP for CO_2 capture in aqueous solution, based on combined QM and classical force field calculations.

C. Protonation tendency of AMP and MEA

To understand why AMP tends to favor the AMP + H_2O → $AMPH^+$ + OH^- reaction, we first examined the interaction of AMP with H_2O by calculating the pairwise distribution function between N in AMP (indicated as N_{AMP}, hereafter) and H in H_2O (H_{H_2O}), with comparison to the pair of N in MEA (N_{MEA}) and H_{H_2O}. Fig. 2 shows the radial distribution functions (RDFs, $g(r)$) for the N_{AMP}–H_{H_2O} and N_{AMP}–H_{H_2O} pairs from AIMD simulations (that were run in the *NVE* ensemble for 5 ps, after equilibrating in the *NVT* ensemble at 330 K for 5 ps). The RDF is given by $g(r) = \langle n(r, r + dr)/4\pi r^2 \rho dr \rangle$, where $n(r, r + dr)$ is the number of atoms in a spherical shell of radius dr (from the reference atom, N) and thickness of dr and ρ is the bulk number density. Here, 30 wt% aqueous AMP (MEA) solution was modeled by placing 3AMP (4MEA) and $32H_2O$ molecules in a cubic periodic box of side 11.27 (11.12) Å; due to the small size of the systems, the RDFs were obtained from the average of 5 cases with different initial configurations for each system.

The small peak at 1.1 Å in the RDF profiles indicates protonation of N_{AMP} (N_{MEA}) through the AMP (MEA) + H_2O → $AMPH^+$ ($MEAH^+$) + OH^- reaction; the relatively larger peak intensity in the AMP case implies its greater tendency to undergo the protonation reaction. This is consistent with the

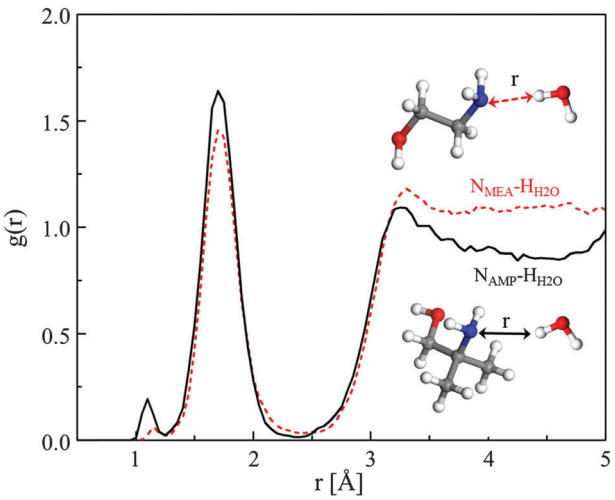

Fig. 2 Radial distribution functions between H in H_2O (H_{H_2O}) and N in MEA (N_{MEA}) (red dotted line) or N in AMP (N_{AMP}) (black solid line) predicted from AIMD simulations at 330 K. The systems consist of $32H_2O$ and 3AMP (4MEA) in a cubic periodic box of side 11.27 Å (11.12 Å), corresponding to approximately 30 wt% aqueous AMP (MEA).

experimentally measured pK_a values of 9.5 in MEA and 9.72 in AMP (in infinitely dilute aqueous solution under standard conditions) that also indicates more favorable protonation of AMP than MEA. Recall that, as mentioned in the introduction, MDEA also preferentially forms HCO_3^-, but at a much lower rate than AMP; this may be because it is less likely to undergo the protonation reaction, indicated by its lower pK_a value of approximately 8.5. The distinct peak at 1.7 Å, attributed to the first nearest neighbor H_{H_2O}, appears to be sharper with higher intensity for AMP compared to MEA. For AMP (MEA), the area under the RDF profile below 2.35 Å (where the minimum is located after the first-nearest neighbor peak) is estimated to be 0.95 (0.93); this value being close to 1 indicates that N in each amine interacts with H_2O by forming a single hydrogen bond. The predicted average distance between N_{AMP} (N_{MEA}) and H_{H_2O} is 1.72 Å (1.74 Å). The shaper RDF peak and the shorter N–H_{H_2O} distance suggest that H_{H_2O} more strongly interacts with N_{AMP} than N_{MEA}. The stronger interaction of N_{AMP}–H_{H_2O} than N_{MEA}–H_{H_2O} tends to enhance the ordering of surrounding H_2O molecules, as demonstrated by the more distinct oscillation in the RDF of AMP after 2.35 Å.

We also performed QM calculations to examine how the presence of CH_3 groups alters the electronic state of N_{AMP}. It has been thought that the higher basicity of AMP is primarily due to electron donation from methyl (CH_3) groups which makes N_{AMP} more negative and polarizable.[47,48] Table 3 shows the calculated CHELPG charges[49] using Gaussian 09 for AMP and MEA in the gas phase, with and without one H_2O molecule interacting with the N of each amine.

The central C atom (C_N) connected to the NH_2 group is predicted to have a charge of $0.585e^-$ ($0.579e^-$) in AMP, compared to $0.285e^-$ ($0.254e^-$) in MEA, for the isolated state (and when interacting with H_2O). N_{AMP} is more negative than N_{MEA} in both cases, and the CH_3 groups have an average charge of approximately $-0.1e^-$ compared to the nearly neutral H's in MEA. The C_N–N distance also elongates to 1.474 Å (in AMP) from 1.464 Å (in MEA). The increase of positive charge on the central C_N atom seems to contradict a simple chemical intuition where CH_3 groups are deemed to have a positive inductive effect (*i.e.*, partial charge release to the C_N atom). We elaborate on this effect by observing that the angles around the central C_N atom slightly increase, suggesting that C_N would presumably change its expected sp^3-like character to a more sp^2-like one.

To further analyze the chemical characteristics of the C_N atom, we used natural bond order analysis (NBO)[50,51] to calculate the hybridizations of C_N and the C_N–R bonds (where R is CH_3 in AMP and H in MEA). The estimated hybridization of C_N is $s^{0.892}p^{2.94}$ in AMP and $s^{1.01}p^{3.16}$ in MEA. The hybridization and electron occupancy (σ) of each individual C–R bond are predicted to be the following:

$$\text{AMP: } C_N sp^{2.17} + C_{CH_3} sp^{2.68} \quad (\sigma = 1.97612)$$

$$\text{MEA: } C_N sp^{3.18} + Hs \quad (\sigma = 1.98836)$$

Table 3 Predicted CHELPG charges and selected distances and angles of (a) AMP and (b) MEA in the gas phase, isolated and with 1 H_2O molecule interacting with N, using QM calculations at a theory level of B3LYP/6-311++G(d,p)

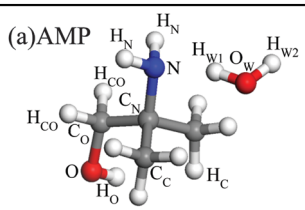

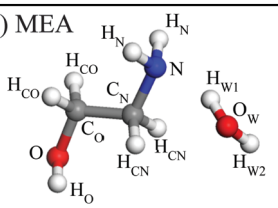

	w/o H_2O	w/H_2O	w/o H_2O	w/H_2O
		Charge [*e*]		
N	−1.008	−0.662	−0.865	−0.624
C_N	0.585	0.579	0.285	0.254
C_O	0.229	0.121	0.194	0.158
C_C	−0.273/−0.269	−0.282/−0.216		
O	−0.644	−0.580	−0.610	−0.601
H_N	0.325/0.325	0.237/0.233	0.313/0.313	0.279/0.279
H_O	0.388	0.369	0.366	0.376
H_{CN}			0.000/−0.004	−0.010/−0.002
H_{CO}	0.035/−0.030	0.026/−0.032	0.037/−0.028	−0.015/0.048
H_C	0.042/0.030/0.063/0.031/0.068/0.067	0.022/0.079/0.050/0.048/0.056/0.052		
O_W		−0.746		−0.717
H_{W1}		0.271		0.267
H_{W2}		0.378		0.351
		Distance [Å]		
C_N–N	1.474	1.484	1.464	1.469
N–H_{W1}		1.952		1.962
O_W–H_{W1}		0.977		0.975
		Angle [°]		
C_O–C_N–C_C/H_{CN}	110/109.9	110.7/110.5	108.6/109.1	108.9/110.1
C_C/H_{CN}–C_N–C_C/H_{CN}	110.3	110.4	106.4	106.5

We can see that the C_N atom in the C–R bond in AMP is more sp^2-like whereas the one in MEA looks much more sp^3-like. This observation is also supported by the electron occupancy analysis showing that the $\sigma(C_N–C_{CH_3})$ bond in AMP has slightly fewer electrons than the $\sigma(C_N–H)$ bond in MEA while deviating more from the ideal value of 2 (which suggests the increased π character of the $C_N–C_{CH_3}$ bond as expected in sp^2 hybridization). This analysis highlights that the steric hindrance due to the CH_3 groups would result in a more planar-like C_N configuration. This in turn causes an electronic redistribution and an increase of effective positive charge on the C_N atom (sp^2 versus sp^3 like carbon) as well as leading to an effectively more negative charge on the N_{AMP} atom and CH_3 groups.

In the presence of H_2O, the $N–H_{H_2O}$ distance slightly decreases to 1.952 Å (in AMP) from 1.962 Å (in MEA) while the H–O bond in H_2O tends to be elongated to 0.977 Å (in AMP) from 0.975 Å (in MEA). This also clearly reflects the stronger interaction of H_2O with N_{AMP} than N_{MEA}. We also estimated the dipole polarizabilities, and the predicted values are $\alpha = 8.74$ Å^3 and 5.35 Å^3 for AMP and MEA, respectively; the larger α may suggest that the protonated AMP can be better stabilized than the protonated MEA, thereby facilitating the AMP + $H_2O \rightarrow AMPH^+ + OH^-$ reaction.

D. Spatial distribution of CO_2 and H_2O around AMP and MEA

Classical MD simulations were performed to examine the distributions of CO_2 and H_2O molecules around AMP and MEA. Fig. 3 shows the pairwise RDFs between N_{AMP} (or N_{MEA}) and H_{H_2O} [(a)] and C_{CO_2} [(b)]; for clarity, corresponding spatial distribution functions (SDFs) [(c)] are also presented. Each system contains 1530H_2O, 170AMP (or MEA) (10 mol%), and 34CO_2 (0.2 moles per mole of amine). The SDFs are calculated similarly to the RDFs, except that the surrounding atoms are not rotationally averaged around the reference atom, and therefore can be used to illustrate where the H_{H_2O} and C_{CO_2} atoms are most likely distributed around N_{AMP}/N_{MEA} in three-dimensional space; that is, the SDF is $g(\vec{r}) = \langle n(\vec{r}, \vec{r} + d\vec{r})/\rho d\vec{r} \rangle$, where $\vec{r}$ is the position of the surrounding atom in Cartesian coordinates from the reference atom N. For the SDF analysis, the simulation box must be rotated around each N so that the surrounding atoms are positioned from a reference orientation of amine; here, the $N–C_N–C_O$ (C attached to the OH group) plane is chosen as the reference. The TRAVIS suite was utilized for the SDF analysis.[52] Both $g(r)$ and $g(\vec{r})$ were averaged from the snapshots generated every 500 fs over a trajectory of 1 ns.

The $N–H_{H_2O}$ RDFs in Fig. 3(a) exhibit similar features as those from AIMD simulations (see Fig. 2). The integrated area under the first peak (up to 2.5 Å) is predicted to be about 1 for both AMP and MEA, reiterating the formation of an $N–H_{H_2O}$ hydrogen bond. As also discussed earlier, the relatively stronger $N_{AMP}–H_{H_2O}$ interaction is well demonstrated by the sharper first neighbor peak and the enhanced short-range order of H_2O molecules around AMP in comparison to the MEA case. This is also supported by the SDFs which show a more localized distribution of H_{H_2O} around N_{AMP} than N_{MEA}; this might also be attributed in part to the bulky methyl groups in AMP which

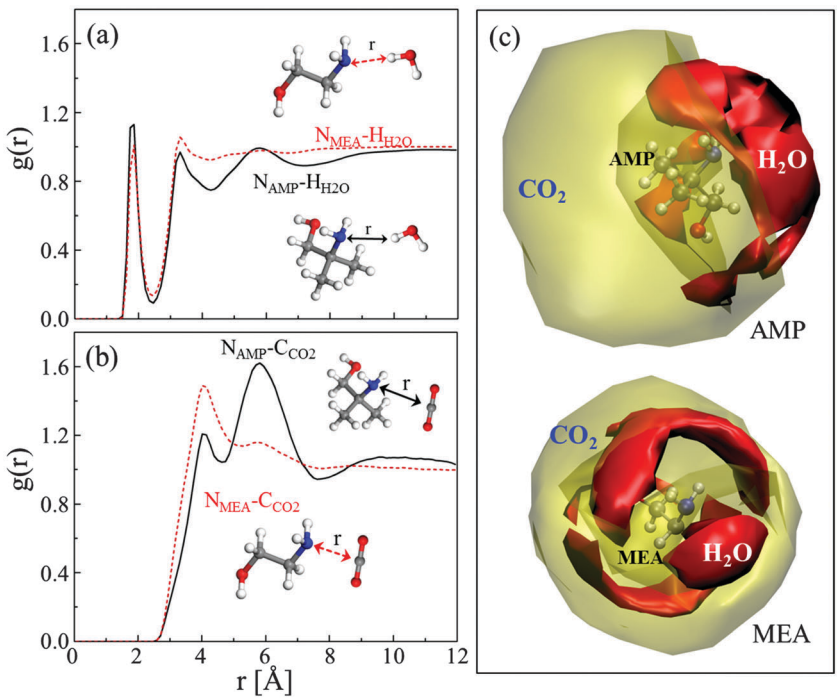

Fig. 3 Radial distribution functions between N in MEA (N_{MEA}) or N in AMP (N_{AMP}) and H in H_2O (H_{H_2O}) [(a)] or C in CO_2 (C_{CO_2}) [(b)] from classical MD simulations performed at 323 K. Spatial distribution functions [(c)] of H_{H_2O} (solid red) and C_{CO_2} (transparent yellow) around N_{AMP}/N_{MEA} were generated using an isosurface threshold of 0.67 and 1.3, respectively. Systems contain 1530H_2O, 34CO_2, 170AMP (MEA) molecules in a cubic simulation box with length 42.04 Å (40.41 Å); this represents 10 mol% aqueous amines with approximately 0.2CO_2 loading (mol CO_2 per mol amine).

may reduce the available volume for H_2O molecules to occupy near the amine group.

To further quantitatively demonstrate how much more the first nearest H_{H_2O} is tightly bound to N_{AMP} compared to N_{MEA}, we also calculated its average residence time from the time correlation function, $C(t) = \langle A(t) \cdot A(0) \rangle / \langle A^2 \rangle$, where $A(t) = 1$ if the original H_{H_2O} is within 2.5 Å (the first minimum in the RDF) and 0 otherwise. As shown in Fig. 4, H_{H_2O} is found to remain longer with N_{AMP} than N_{MEA}; the residence times (τ), obtained by fitting the $C(t)$ profiles to an exponential decay function $\exp[-(t/\tau)]$, are estimated to be 13.6 ps and 6.0 ps respectively in aqueous AMP and MEA.

As shown in Fig. 3(b), the RDF profiles for the $N–C_{CO_2}$ pair exhibit two distinct but overlapping peaks at 4 Å and 6 Å, while the first (second) peak is far more pronounced in the MEA (AMP) case. The farther first peak position compared to the $N–H_{H_2O}$ pair implies that solvation of the N sites may hinder CO_2 accessibility; it is also worthwhile to note that the first peaks for the $N–C_{CO_2}$ pairs coincidence with the first minima of the $N–H_{H_2O}$ cases. The solvation effect tends to be enhanced in the AMP case largely due to the relatively stronger $N_{AMP}–H_{H_2O}$ interaction; that is, enhanced H_2O packing may further suppress CO_2 approaching the N_{AMP} site. The CO_2 distribution around the N site in each system is better illustrated by the SDF isosurface plots in Fig. 3(c), which clearly demonstrate that CO_2 is rather evenly distributed spherically around the N of MEA, whereas it tends to be mostly located near the CH_3 groups of AMP. This implies that in aqueous solution CO_2 may more easily approach the N site of MEA than AMP, thereby facilitating the $2MEA + CO_2 \rightarrow MEACOO^- + MEAH^+$ reaction, whereas the CO_2 reaction with AMP tends to be significantly suppressed by the N site solvation. This analysis highlights that the reaction of CO_2 with aqueous amine can be strongly influenced by the nature of amine solvation, particularly the $N–H_{H_2O}$ hydrogen bonding interaction.

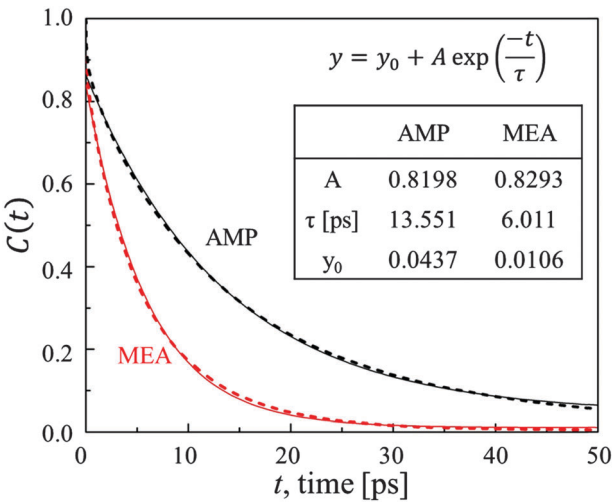

Fig. 4 Time correlation of hydrogen bond between N of AMP (N_{AMP}) or N of MEA (N_{MEA}) and the first nearest neighbor H of H_2O (H_{H_2O}) from classical MD simulations at 323 K (shown as dashed lines) and fitted to exponential decay function (thin solid lines). Systems contain $1530H_2O$, $34CO_2$, 170AMP (MEA) molecules in a cubic simulation box with length 42.04 Å (40.41 Å); this represents 10 mol% aqueous amines with approximately $0.2CO_2$ loading (mol CO_2 per mol amine).

To better understand the role of solvation in the CO_2–AMP reaction, we also performed AIMD simulations with pure AMP at 400 K. In the absence of H_2O, AMP is found to easily react with CO_2 to form $AMPCOO^-$ and $AMPH^+$, *i.e.*, $2AMP + CO_2 \rightarrow AMPCOO^- + AMPH^+$, as illustrated in Fig. S4 (ESI†). Although pure AMP would not be used in a real process, this result supports that the solvation of N sites, rather than the steric hindrance of CH_3 groups, could be mainly responsible for hindering the $2AMP + CO_2 \rightarrow AMPCOO^- + AMPH^+$ reaction. This is consistent with previous experimental studies reporting the formation of $AMPCOO^-$ in some non-aqueous AMP–CO_2 systems.[53]

IV. Conclusions

2-Amino-2-methyl-1-propanol (AMP) and its blends appear to be attractive solvents for CO_2 capture due to their high CO_2 loading capacities and relatively fast absorption rates.[5,6] However, some fundamental aspects of CO_2 absorption mechanisms in AMP-based solutions still remain uncertain. In particular, the reaction of CO_2 with aqueous AMP has been found to preferentially form bicarbonate, whereas MEA and most other primary amines predominantly form carbamate.[11] In this theoretical study, we attempt to elucidate the underlying reason for the preferential production of bicarbonate in aqueous AMP as compared to MEA by explicitly taking into account both thermodynamic and kinetic contributions.

We evaluated the thermodynamic favorability for bicarbonate and carbamate formation by calculating the changes in free energy (and enthalpy) using static QM with an implicit solvent model (and AIMD with explicit solvent). Our calculations show that both CO_2 capture mechanisms are thermodynamically favorable with similar exothermicities in aqueous AMP and MEA solutions. In addition, AIMD simulations demonstrate that AMP carbamate ($AMPCOO^-$) can be as stable as MEA carbamate ($MEACOO^-$) in an aqueous solution, which is consistent with previous theoretical studies predicting large and similar energy barriers for carbamate hydrolysis to form bicarbonate in both cases,[18,20] *i.e.*, $AMPCOO^-$ ($MEACOO^-$) + $H_2O \rightarrow HCO_3^- + AMPH^+$ ($MEAH^+$); the comparable stability between $AMPCOO^-$ and $MEACOO^-$ is also well demonstrated by analysis of the N–C (in CO_2) bonding interaction. This may suggest that the relative concentrations of carbamate and bicarbonate could not be predicted only by their thermodynamic favorability, especially since it may take too long to reach equilibrium at typical operating conditions.

From AIMD simulations, we observed that the $AMP + H_2O \rightarrow AMPH^+ + OH^-$ reaction frequently occurs, rather than carbamate formation (*i.e.*, $2AMP + CO_2 \rightarrow AMPCOO^- + AMPH^+$) which tends to occur readily in the case of MEA. The OH^- may further react with CO_2 to form bicarbonate (*i.e.*, $OH^- + CO_2 \rightarrow HCO_3^-$), as also shown in earlier studies.[40,41] The enhanced AMP protonation reaction is apparently related to its high basicity. Our electronic

structure analysis shows that the steric hindrance of the CH_3 groups of AMP causes a more planar-like configuration around the central C atom (C_N) which is attached to N. The tendency of sp^2-like hybridization results in charge redistribution in which the C_N atom is more positively charged and the N atom is more negatively charged. This in turn strengthens the interaction between the N in AMP and surrounding H_2O molecules while suppressing the accessibility of CO_2 to the N site to form carbamate, relative to the MEA case, as confirmed by analysis of radial/spatial distribution functions from MD simulations. In contrast to the aqueous system, our AIMD simulations also demonstrate that AMP may directly react with CO_2 to form carbamate in the absence of strong solvation, consistent with previous experiments showing carbamate formation in some non-aqueous systems.[53]

Based on our calculation results, we attribute the preferential formation of bicarbonate in CO_2 absorption into an aqueous AMP solution largely to kinetic factors. As discussed above, the strong interaction between N (in AMP) and H (in H_2O) suppresses the reaction with CO_2 and promotes the protonation reaction, while the bicarbonate and carbamate reaction routes exhibit similar thermodynamic favorability. This study highlights that not only thermodynamic but also kinetic factors should be considered in describing the reaction between CO_2 and amines in aqueous solution.

Acknowledgements

This work was supported by the Korea CCS R&D Center (KCRC) grant (No. 2015053544) funded by the Korea government (Ministry of Science, ICT & Future Planning) and the R.A. Welch Foundation (No. F-1535). We would also like to thank the Texas Advanced Computing Center for use of the Stampede supercomputing system (OCI-1134872). Helpful discussions with Gary T. Rochelle and Hoon Sik Kim are also greatly acknowledged.

References

1 E. J. Maginn, *J. Phys. Chem. Lett.*, 2010, **1**, 3478–3479.
2 J. D. Figueroa, T. Fout, S. Plasynski, H. McIlvried and R. D. Srivastava, *Int. J. Greenhouse Gas Control*, 2008, **2**, 9–20.
3 D. Zhu, M. Fang, Z. Lv, Z. Wang and Z. Luo, *Energy Fuels*, 2012, **26**, 147–153.
4 G. S. Goff and G. T. Rochelle, *Ind. Eng. Chem. Res.*, 2004, **43**, 6400–6408.
5 G. Sartori and D. W. Savage, *Ind. Eng. Chem. Fundam.*, 1983, **22**, 239–249.
6 A. K. Chakraborty, G. Astarita and K. B. Bischoff, *Chem. Eng. Sci.*, 1986, **41**, 997–1003.
7 H. Lepaumier, D. Picq and P.-L. Carrette, *Ind. Eng. Chem. Res.*, 2009, **48**, 9061–9067.
8 H. Lepaumier, D. Picq and P.-L. Carrette, *Ind. Eng. Chem. Res.*, 2009, **48**, 9068–9075.
9 M. Caplow, *J. Am. Chem. Soc.*, 1968, **90**, 6795–6803.
10 P. V. Danckwerts, *Chem. Eng. Sci.*, 1979, **34**, 443–446.
11 A. F. Ciftja, A. Hartono and H. F. Svendsen, *Chem. Eng. Sci.*, 2014, **107**, 317–327.
12 J. P. Jakobsen, J. Krane and H. F. Svendsen, *Ind. Eng. Chem. Res.*, 2005, **44**, 9894–9903.
13 T. L. Donaldson and Y. N. Nguyen, *Ind. Eng. Chem. Fundam.*, 1980, **19**, 260–266.
14 P. D. Vaidya and E. Y. Kenig, *Chem. Eng. Technol.*, 2007, **30**, 1467–1474.
15 E. Alper, *Ind. Eng. Chem. Res.*, 1990, **29**, 1725–1728.
16 S.-M. Yih and K.-P. Shen, *Ind. Eng. Chem. Res.*, 1988, **27**, 2237–2241.
17 M. Ismael, R. Sahnoun, A. Suzuki, M. Koyama, H. Tsuboi, N. Hatakeyama, A. Endou, H. Takaba, M. Kubo, S. Shimizu, C. A. Del Carpio and A. Miyamoto, *Int. J. Greenhouse Gas Control*, 2009, **3**, 612–616.
18 H. Yamada, Y. Matsuzaki, T. Higashii and S. Kazama, *J. Phys. Chem. A*, 2011, **115**, 3079–3086.
19 H.-B. Xie, N. He, Z. Song, J. Chen and X. Li, *Ind. Eng. Chem. Res.*, 2014, **53**, 3363–3372.
20 T. Davran-Candan, *J. Phys. Chem. A*, 2014, **118**, 4582–4590.
21 K. Z. Sumon, A. Henni and A. L. L. East, *J. Phys. Chem. Lett.*, 2014, **5**, 1151–1156.
22 G. Kresse and J. Furthmuller, *Phys. Rev. B: Condens. Matter Mater. Phys.*, 1996, **54**, 11169–11186.
23 J. P. Perdew, K. Burke and M. Ernzerhof, *Phys. Rev. Lett.*, 1996, **77**, 3865–3868.
24 M. J. Frisch, G. W. Trucks, H. B. Schlegel, G. E. Scuseria, M. A. Robb, J. R. Cheeseman, G. Scalmani, V. Barone, B. Mennucci, G. A. Petersson, H. Nakatsuji, M. Caricato, X. Li, H. P. Hratchian, A. F. Izmaylov, J. Bloino, G. Zheng, J. L. Sonnenberg, M. Hada, M. Ehara, K. Toyota, R. Fukuda, J. Hasegawa, M. Ishida, T. Nakajima, Y. Honda, O. Kitao, H. Nakai, T. Vreven, J. A. Montgomery, J. E. Peralta, F. Ogliaro, M. Bearpark, J. J. Heyd, E. Brothers, K. N. Kudin, V. N. Staroverov, T. Keith, R. Kobayashi, J. Normald, K. Raghavachari, A. Rendell, J. C. Burant, S. S. Iyengar, J. Tomasi, M. Cossi, N. Rega, J. M. Millam, M. Klene, J. E. Knox, J. B. Cross, V. Bakken, C. Adamo, J. Jaramillo, R. Gomperts, R. E. Stratmann, O. Yazyev, A. J. Austin, R. Cammi, C. Pomelli, J. W. Ochterski, R. L. Martin, K. Morokuma, V. G. Zakrzewski, G. A. Voth, P. Salvador, J. J. Dannenberg, S. Dapprich, A. D. Daniels, O. Farkas, J. B. Foresman, J. V. Ortiz, J. Cioslowski and D. J. Fox, *Gaussian 09 Revis. C.01*, Gaussian, Inc., Wallingord CT, 2010.
25 A. V. Marenich, C. J. Cramer and D. G. Truhlar, *J. Phys. Chem. B*, 2009, **113**, 6378–6396.
26 S. Plimpton, *J. Comput. Phys.*, 1995, **117**, 1–19.
27 E. F. da Silva, T. Kuznetsova, B. Kvamme and K. M. Merz Jr., *J. Phys. Chem. B*, 2007, **111**, 3695–3703.
28 W. D. Cornell, P. Cieplak, C. I. Bayly, I. R. Gould, K. M. Merz Jr., D. M. Ferguson, D. C. Spellmeyer, T. Fox, J. W. Caldwell and P. A. Kollman, *J. Am. Chem. Soc.*, 1995, **117**, 5179–5197.
29 H. J. C. Berendsen, J. R. Grigera and T. P. Straatsma, *J. Phys. Chem.*, 1987, **91**, 6269–6271.
30 S.-N. Huang, T. A. Pascal, W. A. Goddard, P. K. Maiti and S.-T. Lin, *J. Chem. Theory Comput.*, 2011, **7**, 1893–1901.
31 J. G. Harris and K. H. Yung, *J. Phys. Chem.*, 1995, **99**, 12021–12024.

32 C. I. Bayly, P. Cieplak, W. D. Cornell and P. A. Kollman, *J. Phys. Chem.*, 1993, **97**, 10269–10280.
33 J.-P. Ryckaert, G. Ciccotti and H. J. C. Berendsen, *J. Comput. Phys.*, 1977, **23**, 327–341.
34 U. Essmann, L. Perera, M. L. Berkowitz, T. Darden, H. Lee and L. G. Pedersen, *J. Chem. Phys.*, 1995, **103**, 8577–8593.
35 W. G. Hoover, *Phys. Rev. A: At., Mol., Opt. Phys.*, 1985, **31**, 1695–1697.
36 H. Arcis, L. Rodier and J.-Y. Coxam, *J. Chem. Thermodyn.*, 2007, **39**, 878–887.
37 H. Arcis, K. Ballerat-Busserolles, L. Rodier and J.-Y. Coxam, *J. Chem. Eng. Data*, 2011, **56**, 3351–3362.
38 *CRC Handbook of Chemistry and Physics*, ed. W. M. Haynes, CRC Press/Taylor and Francis, Boca Raton, FL, 96th edn, 2015, Internet Version 2016.
39 C. P. Kelly, C. J. Cramer and D. G. Truhlar, *J. Phys. Chem. A*, 2006, **110**, 2493–2499.
40 K. Leung, I. M. B. Nielsen and I. Kurtz, *J. Phys. Chem. B*, 2007, **111**, 4453–4459.
41 A. Stirling, *J. Phys. Chem. B*, 2011, **115**, 14683–14687.
42 H.-B. Xie, J. K. Johnson, R. J. Perry, S. Genovese and B. R. Wood, *J. Phys. Chem. A*, 2011, **115**, 342–350.
43 P. Jackson, *Struct. Chem.*, 2014, **25**, 1535–1546.
44 G. S. Hwang, H. M. Stowe, E. Paek and D. Manogaran, *Phys. Chem. Chem. Phys.*, 2015, **17**, 831–839.
45 D. Asthagiri, L. R. Pratt, J. D. Kress, M. A. Gomez and M. A. Ratner, *Proc. Natl. Acad. Sci. U. S. A.*, 2004, **101**, 7229–7233.
46 E. F. da Silva and H. F. Svendsen, *Int. J. Greenhouse Gas Control*, 2007, **1**, 151–157.
47 H. Umeyama and K. Morokuma, *J. Am. Chem. Soc.*, 1976, **98**, 4400–4404.
48 A. K. Chakraborty, K. B. Bischoff, G. Astarita and J. R. Damewood Jr., *J. Am. Chem. Soc.*, 1988, **110**, 6947–6954.
49 C. M. Breneman and K. B. Wiberg, *J. Comput. Chem.*, 1990, **11**, 361–373.
50 J. P. Foster and F. Weinhold, *J. Am. Chem. Soc.*, 1980, **102**, 7211–7218.
51 A. E. Reed, R. B. Weinstock and F. Weinhold, *J. Chem. Phys.*, 1985, **83**, 735–746.
52 M. Brehm and B. Kirchner, *J. Chem. Inf. Model.*, 2011, **51**, 2007–2023.
53 H. Svensson, J. Edfeldt, V. Z. Velasco, C. Hulteberg and H. T. Karlsson, *Int. J. Greenhouse Gas Control*, 2014, **27**, 247–254.

